A Combustion Model Sensitivity Study for CH_4/H_2 Bluff-Body Stabilised Flame

M Hossain

School of Engineering, The Robert Gordon University,
Schoolhill, Aberdeen, AB15 9QE

Phone: 01224 262351 Fax: 01224 262444
Email: M.Hossain@rgu.ac.uk

W Malalasekera

Wolfson School of Mechanical and Manufacturing Engineering
Loughborough University, Leicestershire, LE11 3TU, UK

Phone: 01509 227556, Fax: 01509 227648
Email: W.Malalasekera@lboro.ac.uk

Abstract

The objective of this work is to assess the performance of different combustion models in predicting turbulent nonpremixed combustion in conjunction with the $k-\varepsilon$ turbulence model. The laminar flamelet, equilibrium chemistry, constrained equilibrium chemistry and flame sheet models are applied to simulate combustion in a CH_4/H_2 bluff-body flame experimentally studied by the University of Sydney. The computational results are compared to experimental values of mixture fraction, temperature and constituent mass fractions. The comparison shows that the laminar flamelet model performs better than other combustion models and mimics most of the significant features of the bluff body flame.

Keywords: laminar flamelet, nonpremixed, combustion

NOMENCLATURE

C_{g1}, C_{g2}	model constant in the mixture fraction variance equation
C_P	specific heat of mixture
$C_{\varepsilon 1}$, $C_{\varepsilon 2}$, C_μ	turbulence model constant
C_χ	constant in the scalar dissipation rate equation
D	diameter
G	turbulence production
H_{fu}	heating value of fuel
k	turbulence kinetic energy
m	mass fraction of species
$P()$	probability density function
P	pressure
s	stoichiometric mass of oxygen to burn 1 kg of fuel
u_j	velocity vector
x	axial location
x_i, x_j	distance vector
Z	mixture fraction
$\widetilde{Z}^{"2}$	mixture fraction variance

Greek

χ	scalar dissipation rate
ε	turbulent energy dissipation rate
ϕ	scalar variables
μ_{eff}	effective viscosity
μ_t	turbulent viscosity
ρ	density
σ_k, σ_ε	turbulence model constant

σ_t	turbulent Prandtl number
σ_χ^2	standard deviation of the log-normal distribution

Subscript

A	air stream
fu	fuel
F	fuel stream
ox	oxygen
ref	reference temperature
st	stoichiometric

Superscripts

$\bar{}$	conventional ensemble average
$\tilde{}$	density-weighted ensemble average
$''$	density-weighted fluctuation

1 INTRODUCTION

Development of combustion models for turbulent nonpremixed flames has attracted significant attentions owing to the frequent occurrences of nonpremixed combustion in a wide range of practical combustion systems. To achieve accurate prediction of thermochemical properties of a turbulent flame, the relevant physical processes such turbulence, chemical kinetics and turbulence-chemistry interaction have to be properly represented. The turbulent transport of mass, momentum and energy in practical flows can be represented by a first-order closure based on a gradient transport assumption. However, the closure of mean chemical reaction in the species transport equation requires higher level correlations, making it practically impossible to determine in turbulent combustions. This has led to the development of alternative approaches to the modelling of nonpremixed flames with different level of complexities. The fast chemistry based models include the conserved scalar model with either the flame sheet or equilibrium chemistry [1], and the eddy breakup model [2]. The conserved scalar model is based on the instantaneous relationship of the thermo-chemical properties of the flame as a function of the mixture fraction (conserved scalar). The influence of turbulence is accounted for by a presumed probability distribution of the mixture fraction. The eddy break up model defines the rate of chemical reaction by the rate of turbulent mixing of fuel and oxidizer eddies. One of the shortcomings of this model is that the model parameters have to be adjusted depending on the type of fuel and combustion systems [3, 4]. Advanced combustion models, which are capable of accounting for turbulence-chemistry interaction and nonequilibrium effects are the laminar flamelet model [5,6], the conditional moment closure model [7] and the PDF transport model [8, 9]. The laminar flamelet model considers a turbulent flame as an ensemble of laminar flamelets, which are strained by turbulence. A laminar flamelet structure can be obtained from a one-dimensional laminar counterflow simulation or a flamelet equation on the mixture fraction space derived by co-ordinate transformation. A flamelet library which comprises of a set of flamelet profiles can be constructed in terms of instantaneous mixture fraction and scalar dissipation rate. The average scalar properties in a turbulent flame can be computed by integrating the laminar flamelet library with a probability density function of the mixture fraction and the scalar dissipation rate. This model thus decouples the turbulent flow field calculation from

the chemistry calculation and hence allows the incorporation of complex chemical kinetics in turbulent nonpremixed flame calculation. The conditional moment closure (CMC) model is based on the statistical conserved scalar approach, where conditional average equations for random reacting scalars are solved. The closure of the mean reaction term is obtained by the first or higher order conditional moments of the reactive scalars in the Arrheneous reaction rate. The CMC model has been shown to provide good results if the relevant conditional means are properly modelled [10]. However, the CMC model is computationally expensive specially if the number of chemical species is large. The PDF-transport model is theoretically the most advanced model and is capable of handling the reaction rate term without any modelling assumption. The accuracy of the model is however dependent on the appropriate modelling of the mixing rate. The proper modelling of this term has led to this model being cable of modelling of such complex issues as different levels of local extinction. On the downside, the transported pdf model is computationally very expensive. The application of the CMC and the transported PDF models for practical design is not widespread. The flame sheet, the eddy break up and the laminar flamelet models are currently the viable option for industrial applications. The objective of this work is to provide an assessment of the conserved scalar based flame sheet, equilibrium and the laminar flamelet model which are simpler to implement and faster to execute and hence are more suitable for industrial applications.

The bluff-body combustor provides an ideal geometry for the combustion model evaluation as the bluff-body geometry provides well defined initial and boundary conditions. The bluff-body geometry also provides some complexities of an industrial combustor with its recirculation zone. The main fuel steam and the coflow air stream enter the bluff-body combustor separately and create recirculation zones at the face of the bluff body. The recirculation zone contains hot products which act as an ignition source. The recirculation zone helps to stabilise the flame at the face of the bluff body. The zone downstream of the recirculation zone is called neck zone which encounters intense turbulent mixing. This is an ideal location for evaluating the combustion models for turbulent-chemistry interaction. Further downstream, the fuel and air jet merge to form a jet like zone. The bluff-body flame studied here was one of the target flames in the International Workshop on Measurement and Computation of Turbulent Nonpremixed flames (TNF Workshop) [11]. It was experimentally

studied by Dally et al [12] and the experimental data has been made available from the University of Sydney website [13]. The same flame has been studied numerically by a number of researchers focusing on either combustion or turbulence model. Dally et al [14] reported simulation results obtained using standard and modified $k-\varepsilon$ and Reynolds stress models for turbulence and flame sheet model with beta probability density function for combustion. The main focus of their work was on the prediction of flow field, and both the $k-\varepsilon$ and Reynolds stress models in the standard form failed to predict the flow field sufficiently accurately. The value of turbulence model constant of $C_{\varepsilon 1}=1.6$ was proposed to improve the prediction of the flow field.. Merci et al [15] applied a new cubic nonlinear eddy viscosity turbulence model with a constrained equilibrium model to predict this flame. Their prediction showed that the improvements in flow field prediction using the new cubic model was only modest. As a result, the prediction of temperature profiles at downstream locations were not good. Li et al [16] investigated this flame using various differential Reynolds stress models with the equilibrium chemistry model. They reported that all the differential stress models in the standard form failed to reproduce the mean velocity, velocity fluctuations, mean mixture fraction and its variences. Modification to turbulence model constant led to minor improvements of the mean mixture fraction and variance profiles in upstream locations. However, the mean mixture fraction profiles were severely underpredicted at downstream locations. Their reported temperature prediction showed underprediction near the fuel jet and this shortcoming was attributed to the shortcomings of the equilibrium chemistry model. Yan et al [17] provided a turbulence model sensitivity study using the standard $k-\varepsilon$ model, the explicit algebraic stress model and the $k-\varepsilon$ model with varied anisotropy parameter together with a steady laminar flamelet model. Their study provided a very good prediction of mixture fraction profiles at upstearm locations, though there was slight overprediction near the centreline. The mixture fraction profiles were underpredicted further downstream locations. The prediction of mixture fraction variances as well as velocity fluctuations was not good. Despite this, temperature and major species were well predicted in their study. It is noteworthy that almost all of the approaches mentioned above needed modifications to the standard value of the model constants to provide a good prediction. The same bluff body flame was also modelled by a conditional moment closure model using GRI Mech 2.11, 3.0 and Miller-Bowman

mechanisms by Kim et al [10]. They employed $k-\varepsilon$ turbulence model with $C_{\varepsilon 1}=1.6$. Their calculation showed good prediction of mean velocity and mixture fraction, however, the prediction of fluctuations of velocity and mixture fraction were not that good. Major species as well as temperature were well predicted but the NO was overpredicted and the level of overprediction was particularly high with GRI Mech 3.0 mechanism. Previous predictions of this bluffbody flame with a laminar flamelet model by Hossain and Malalasekera [18, 19], a coupled radiation/flamelet combustion model by Hossain et al [20] showed reasonably good prediction at the upstream locations. The PDF transport model by Muragoglu et al. [21] utilised a joint velocity-turbulent frequency-compositions pdf with chemistry represented by a laminar flamelet concept to model this flame. Their PDF method predicted the flow field and the mean scalar field very well inside the recirculation zone, however, the prediction deteriorated further downstream. They did not report the prediction of temperature or species concentrations. Liu et al [22] reported prediction of the same flame with a joint PDF model with detailed chemistry. Their prediction showed poor agreement in the downstream locations. At upstream locations their predictions of temperature and species concentrations were generally quite good.

The bluff-body flame of the present study showed minor departure from chemical equilibrium. All previous computational studies [14-17] based on fast chemistry model did not produce a comprehensive report on the performance of combustion models by comparing all the major and minor species. These studies mainly concentrated on the effect of turbulence modelling on the flow field. On the other hand, the modelling study based on advanced combustion models [10,18-22] was more extensive in comparing temperature and major and minor species. The present study seeks to provide a comprehensive comparison of the most commonly available combustion models, such as flame sheet, equilibrium, constrained equilibrium and the laminar flamelet models, in commercial codes FLUENT and CFX

2 COMPUTATIONAL DETAILS

The numerical model of turbulent combustion is formulated from the Favre-averaged Navier-Stokes equation together with turbulence and combustion models. Favre-averaged Navier-Stokes equation can be expressed in Cartenian tensor notation as:

$$\frac{\partial \overline{\rho}\widetilde{u}_j}{\partial x_j} = 0 \tag{1}$$

$$\frac{\partial}{\partial x_j}\left(\overline{\rho}\widetilde{u}_j\widetilde{u}_i\right) = -\frac{\partial P}{\partial x_i} + \mu_{eff}\frac{\partial}{\partial x_j}\left(\frac{\partial u_j}{\partial x_i} + \frac{\partial u_i}{\partial x_j}\right) \tag{2}$$

where μ_{eff} is effective viscosity given by $\mu_{eff} = \mu + \mu_t$

The eddy viscosity μ_t is given by

$$\mu_t = \overline{\rho}C_\mu \frac{\widetilde{k}^2}{\widetilde{\varepsilon}}$$

In the present study, the $k-\varepsilon$ turbulence model is used for accounting the turbulence fluctuations in the flow field. The equation used to model turbulence kinetic energy, k is of the form:

$$\frac{\partial}{\partial x_j}\left(\overline{\rho}\widetilde{u}_j\widetilde{k}\right) = \frac{\partial}{\partial x_j}\left(\frac{\mu_t}{\sigma_k}\frac{\partial \widetilde{k}}{\partial x_j}\right) + G - \varepsilon \tag{3}$$

where G is turbulence production due to strain and is given by:

$$G = \mu_t\left(\frac{\partial \widetilde{u}_i}{\partial x_j} + \frac{\partial \widetilde{u}_j}{\partial x_i}\right)\frac{\partial \widetilde{u}_i}{\partial x_j}$$

The transports equation for the dissipation of turbulent kinetic energy ε is of the form:

$$\frac{\partial}{\partial x_j}\left(\bar{\rho}\tilde{u}_j\tilde{\varepsilon}\right)=\frac{\partial}{\partial x_j}\left(\frac{\mu_t}{\sigma_\varepsilon}\frac{\partial\tilde{\varepsilon}}{\partial x_j}\right)+C_{\varepsilon 1}\frac{\tilde{\varepsilon}}{\tilde{k}}G-C_{\varepsilon 2}\bar{\rho}\frac{\tilde{\varepsilon}^2}{\tilde{k}} \tag{4}$$

The model constants C_μ, $C_{\varepsilon 1}$, $C_{\varepsilon 2}$, σ_k, σ_ε have the values 0.09, 1.60, 1.92, 1.3 and 1.0 respectively. The value of $C_{\varepsilon 1}$ is modified from the standard value of 1.44 to 1.60 following the work of Dally et al. [**14**] and Hossain et al. [**20**]. The value of $C_{\varepsilon 1}=1.60$ is also recommended for bluff body flames by the "International Workshop on Measurements and Computations of Turbulent Nonpremixed Flames (TNF)" .

2.1 The Conserved scalar model

The thermo-chemical properties within a nonpremixed combustion systems can be related to a single conserved scalar, the mixture fraction. Thermo-chemical models are then required to specify the relationship between the mixture fraction and the scalar variables. In the present study the flame sheet, equilibrium and constrained equilibrium models are implemented to describe the relationship between the scalar variables with the mixture fraction. These models are based on fast chemistry, where time required to complete reaction is much shorter than the convection and diffusion time in a turbulent flame.

The Flame sheet model

The flame sheet model assumes that the chemical reaction takes place in a single irreversible step at a thin flame sheet. The flame sheet is located at the stoichiometric mixture fraction. Outside the flame sheet, inert mixing between reactants and products take place. In the flame sheet model, the mass fractions of fuel and oxidant are given by [1]

$$m_{fu} = m_{fu,F} \max\left(\frac{Z - Z_{st}}{1 - Z_{st}}, 0\right) \tag{5}$$

$$m_{ox} = m_{ox,A} \max\left(\frac{Z_{st} - Z}{Z_{st}}, 0\right) \tag{6}$$

where, Z_{st} is stoichiometric mixture fraction defined by

$$Z_{st} = \frac{m_{ox,A}}{s m_{fu,F} + m_{ox,A}} \tag{7}$$

the subscripts A and F refer to air and fuel stream respectively, s is stoichiometric mass of oxygen.

The temperature is obtained from

$$\int_{T_{ref}}^{T} C_p dT = h(Z) - m_{fu} H_{fu} \tag{8}$$

where C_p refers to the specific heat of the mixture, H_{fu} is the heating value of fuel. The density is obtained from the ideal gas law.

The equilibrium model

At high temperature, the flame combustion does not proceed to a completion, and some reactions occur in reverse direction. When the rate of reverse reaction equals the rate of forwards one a chemical equilibrium is reached. The equilibrium composition and temperature of the flame can be calculated as a function of the mixture fraction based on Gibbs free energy [23]. A dedicated computer program can be employed to predict equilibrium species concentrations and temperature. In the present study, the pre-pdf code of FLUENT is used for the equilibrium calculation. A constrained

equilibrium composition is also calculated using the same code. In this method, the equilibrium calculation is restricted upto a rich flammability limit. This is because the equilibrium model predicts the endothermic breakdown of hydrocarbon fuel into CO and H_2; but in reality, chemical kinetic mechanisms to achieve this conversion are very slow or nonexistent.

The presumed pdf method

Nonlinearity of the instantaneous relationship between the mixture fraction and the scalar variables $\phi(Z)$ implies that the mean scalar variables in a turbulent field can not be obtained from $\tilde{\phi} = \phi(\tilde{Z})$. The mean scalar variables in a turbulent field are thus obtained introducing a probability density function $P(Z)$:

$$\tilde{\phi} = \int_0^1 \phi(Z) P(Z) dZ \tag{9}$$

The probability density function $P(Z)$ is assumed as a beta distribution and the $P(Z)$ is constructed from transport equations of the mean mixture fraction, $\tilde{Z}$ and the mixture fraction variance, $\tilde{Z}^{"2}$:

$$\frac{\partial}{\partial x_j}\left(\bar{\rho}\tilde{u}_j\tilde{Z}\right) = \frac{\partial}{\partial x_j}\left(\frac{\mu_t}{\sigma_t}\frac{\partial \tilde{Z}}{\partial x_j}\right) \tag{10}$$

$$\frac{\partial}{\partial x_j}\left(\bar{\rho}\tilde{u}_j\tilde{Z}^{"2}\right) = \frac{\partial}{\partial x_j}\left(\frac{\mu_t}{\sigma_t}\frac{\partial \tilde{Z}^{"2}}{\partial x_j}\right) + C_{g1}\mu_t\left(\frac{\partial \tilde{Z}^{"2}}{\partial x_j}\right)^2 - C_{g2}\frac{\tilde{\varepsilon}}{\tilde{k}}\bar{\rho}\tilde{Z}^{"2} \tag{11}$$

where $\sigma_t = 0.7$ and the constants $C_{g1} = 2.8$ and $C_{g2} = 2.0$.

In the CFD code, transport equations are solved for the mean mixture fraction $\tilde{Z}$ and mixture fraction variance $\tilde{Z}''^2$. The mean and variance of the mixture fraction completely describe the beta function.

2.2 Laminar flamelet model

The laminar flamelet model views the turbulent flame as an ensemble of laminar flamelet structures, which are corrugated by the action of turbulent fluctuations [5, 6]. The laminar flamelet modelling of turbulent combustion is a two-step process. In the first step, a laminar flamelet library is calculated by solving governing equations for a counterflow diffusion flame. As the flow is laminar, a detailed chemical reaction mechanism and a realistic transport properties can be prescribed for calculating the flamelet library. In the second step, the flamelet profiles are used as an input data to a CFD code, which calculates the mean scalar variables in a turbulent combustion.

The flamelet profiles specify temperature, density and species concentrations by the mixture fraction and the scalar dissipation rate. For turbulent flames, the mean scalar variables are computed from the laminar flamelet relation of the mixture fraction and the scalar dissipation rate by integrating over a joint probability density function as

$$\tilde{\phi} = \int_0^\infty \int_0^1 \phi(Z,\chi) P(Z,\chi) dZ d\chi \qquad (12)$$

The assumption of statistical independence leads to $P(Z,\chi) = P(Z)P(\chi)$ [5].

The mean value of the scalar dissipation rate can be modelled as

$$\tilde{\chi} = C_\chi \frac{\tilde{\varepsilon}}{\tilde{k}} \tilde{Z}''^2 \qquad (13)$$

where $\tilde{k}$ and $\tilde{\varepsilon}$ are the mean turbulence kinetic energy and energy dissipation rate respectively and C_χ is a constant set equal to 2.0 [**5**]. The distribution of the scalar dissipation rate, $P(\chi)$, is assumed to be log-normal [**5**]. The standard deviation for the log-normal distribution of the scalar dissipation rate is set equal to $\sigma_\chi^2 = 2.0$ [**5**].

The laminar flamelet model requires a library of flamelets. The flamelet library is generated for one dimensional counterflow diffusion flame using RUN-1DL code [**24**]. The flamelet profiles obtained in the physical space are converted into the mixture fraction space by using Bilger formula for mixture fraction [**25**]. The chemical mechanism used to generate flamelet profiles comprises of 16 species and 40 reaction steps. The reaction mechanism is known as Warnatz's mechanism and is taken from the reference [**26**]. During the generation of flamelet library, the differences in molecular diffusivities and hence non-unity Lewis number can be included. In turbulent flames, the diffusion of individual species will be dependent on the turbulent diffusion rather than the molecular diffusion. Dally et al [12] have shown that there is little or no differential diffusion effects for this flame. Accordingly, it is much more realistic to compare turbulent flame composition with those flamelets computed with the unity Lewis number assumption. Hossain and Malalasekera [**19**] have also reported that the unity Lewis number provides better representation of the molecular diffusion of the species for this flame. The flamelet library comprises of 7 libraries for the scalar dissipation rate of 0.06, 0.43, 2.14, 10.69, 21.31, 38.50 /s (extinction limit) and an extinguished flamelet represented by the pure mixing or air and fuel.

3 PROBLEM CONSIDERATION

3.1 Experimental configuration

The case considered here has been experimentally studied at the University of Sydney. The schematic drawing of the bluff-body flame is shown in Figure 1. The fuel is released through a 3.6 mm opening of a 50 mm diameter solid cylinder, which is surrounded by an outer tube supplying coflow air. Experimental results for a variety of test cases with different fuel composition and fuel velocity are available from the

University of Sydney web site. The experimental data used in this work is for CH_4/H_2 fuel with the fuel velocity of 118 m/s and coflow air velocity of 40 m/s. This flame is designated as the HM1 flame.

3.2 Computational details

An existing finite volume in-house CFD code has been used for solving the governing differential equations. The existing CFD code has been modified to include the flame sheet, equilibrium, constrained equilibrium and laminar flamelet models. The 2D axi-symmetric computational domain extends 170 mm in the radial direction and 216 mm direction. A 99 (axial) x 89 (radial) grid arrangement has been used in the calculation. A fully developed velocity and turbulence properties have been specified at the inlet section calculated separately for annular pipe.

4 RESULT AND DISCUSSIONS

Mean axial and radial velocity profiles are shown in Figures 2 and 3. The axial velocity is well predicted. The mean radial velocity is also well reproduced except at x/D=1.8. The mean radial velocity measurement shows some scatter, and the discrepancy may be attributed to the inaccuracies in the radial component measurements as discussed in reference [14]. Figures 2 and 3 also show results obtained with two different grids. The velocity profiles are not influenced by the refinement of the grid. Therefore, a 99 (axial) x 89 (radial) grid is used for all subsequent calculations. The rms values of the axial velocity fluctuations are shown in Figure 4. The predicted results are qualitatively comparable with the measurements.

Figure 5 shows the computed mean mixture fraction profiles compared with the experimental data at different axial locations. In general, the numerical results from all the models are very similar except near the axis. The predicted profiles agree well

with the experimental results in the upstream locations up to $x/D = 1.3$. At $x/D = 1.8$ and $x/D = 2.4$, all the models underpredict the mixture fraction. This can be attributed to the shortcomings of the $k-\varepsilon$ model, which is known to overpredict the decay rate of jet. The modification to the value of C_μ from 1.44 to 1.60 has provided better prediction except at these two locations.

Figure 6 shows the radial profiles of variance of the mixture fraction. The variance of the mixture fraction prediction is not as good as the mean mixture fraction profiles by all combustion models. A closer look, however, shows that the laminar flamelet model provides a slightly better prediction in the upstream locations up to $x/D = 0.9$.

The mean temperature profiles are presented in Figure 7. This figure shows that predicted different temperature profiles are very different for various combustion models. The flame sheet model overpredicts the temperature field, whereas the equilibrium model produces unrealistic profile in the fuel rich zone especially at the first three measurement stations. At $x/D = 0.6$, the peak temperature prediction shows large underprediction. At this location, the flame was subjected to intense mixing of air and fuel resulting in large scale unsetadiness and local extinction [14]. Since none of the model can handle local extinction, the temperature profile is overpredicted at this location by all the models. All previous studies of this flame also provided overprediction at this location. At $x/D = 1.8$ and $x/D = 2.4$, the overprediction of temperature near the centreline by all the combustion models has been caused by the underprediction of the mean mixture fraction profile.

Figures 8 and 9 show mass fraction of the fuel components CH_4 and H_2 respectively. The mass fraction profile of CH_4 has been well predicted by all combustion models, except the equilibrium model. At all measuring stations, the mass fraction of CH_4 has been underpredicted by the equilibrium model. In the equilibrium model, CH_4 breakdowns in the fuel rich zone resulting in the underprediction CH_4 and overprediction of H_2

Figure 10 shows that computed mass fraction of H_2O is well reproduced by the flame sheet model, the constrained equilibrium model and the laminar flamelet model. The

equilibrium model produces underprediction with unrealistic double peak in the profile. This underprediction is a result of producing excess amount of H_2..

The radial mass fraction of profiles of CO_2 is shown in Figure 11. The laminar flamelet model captures the CO_2 profile reasonably accurately except at $x/D = 1.8$ and $x/D = 2.4$. The other models have produced less satisfactory prediction compared to H_2O prediction. The flame sheet model overpredicts the CO_2 severely, the constrained equilibrium prediction is reasonably good, whereas, the equilibrium model again produced the unrealistic double peak in the upstream locations of the flame ($x/D \leq 0.9$).

Radial profiles of mass fraction of OH are shown in Figure 12. Radical OH is formed through the rapid two-body reaction $H+O_2=OH+O$. The OH concentration decays towards the equilibrium via the slower three-body recombination reaction $H+OH+M=H_2O+M$ [27, 28]. In turbulent reacting flows, the rate of mixing is much slower than the chemical reaction of the two-body reaction, but much faster than the three-body reaction [28]. This results in superequilibrium amount of OH in the upstream of the flame, which gradually diminishes to the equilibrium amount further downstream. So, the prediction of OH is a good indication of the predictive capability of the models for nonequilibrium effects. The laminar flamelet model successfully reproduced the super equilibrium amount of OH in the near burner region and the gradual decay towards the equilibrium level. The prediction by the equilibrium and the constrained equilibrium model is almost identical and as expected both models underpredict the OH level in the near burner region. The level of underprediction gradually decreases further downstream in the neck zone.

Radial profiles of CO mass fraction is shown in Figure 13. The flame sheet model, which assumes the chemical reaction takes place in a one step reaction producing final products, obviously cannot compute the intermediate species CO. The equilibrium model severely overpredicts the CO level at all measuring locations. The constrained equilibrium model prediction is somewhat better, but it still overpredicts the CO level. The flamelet model yields prediction with the closest agreement with the experimental data. At $x/D = 1.8$ and $x/D = 2.4$, where the predictions for the

mixing field are worse, the mean CO prediction is very good. At these locations, the under predictions of the mixture fraction should lead to overprediction of CO, whereas the overprediction of mixture fraction variance (specially near the centre line) should lead to underprediction of CO. The relatively best agreement found for the CO at these two stations may be caused by the cancellation of errors in the mean and variance of mixture fraction.

5 CONCLUSION

A bluff-body stabilised CH_4/H_2 nonpremixed flame has been numerically investigated in order to analyse the capability of the flame sheet, equilibrium, constrained equilibrium and the laminar flamelet model. The turbulence has been modelled with a $k-\varepsilon$ model with the model constant $C_{\varepsilon 1}=1.60$.

The level of agreement between measurements and predictions in reacting flows is influenced by turbulence model and combustion model. Therefore the conclusions on performance of combustion models are valid when there is good agreement in the flow fields such as the mean mixture fraction and mixture fraction fluctuations. In the present study, all the combustion models produced similar mixture fraction profiles, but different mixture fraction variances, which might be caused by the difference in computation of density field. Overall the agreement between computations and measurements has been better in the upstream zone of the flame $x/D \le 1.3$ and the final conclusion on the performance of the combustion models has been drawn at these locations. All previous studies of the same flame by other researchers using more complex RSM and DS turbulence models failed to predict accurately the mean mixture fraction and mixture fraction fluctuations beyond $x/D=1.3$. Therefore, the performance of the models in the neck zone of around $x/D=1.8$,where more intense mixing of fuel and air takes place, could not be analysed with greater certainty.

The flame sheet model can only predict major species and it provided good prediction for temperature and mass fraction of H_2O. However, it overpredicted the CO_2 level.

The constrained equilibrium model provided good prediction for temperature, CO_2, H_2O, underprediction for OH level and overprediction for CO level. The equilibrium model, on the other hand, provided poor prediction for temperature and species mass fractions. In the present study, only the laminar flamelet model provided good prediction for temperature and mass fraction of major and minor species. The agreement achieved is the present study is comparable with those in previous reported studies [10, 21-22]. Therefore, it can be concluded that even for the flame that is far away from local extinction, inclusion of advanced chemistry model is required to capture all the combustion features.

6 REFERENCE

1. **Jones, W. P. and Whitelaw, J. H.** Calculations method for reacting turbulent flows: a review. *Combust. And Flame*, 1982, **48**, 1-26.
2. **Magnussen, B. F. and Hjertager, B. H.** On modelling of turbulent combustion with special emphasis on soot formation and combustion. *Proc. Combust. Inst.*, 1976, **18**, 719-729.
3. **Visser, B. M., Smart, J. P., Van de Kamp, W. L. and Weber, R**. Measurements and predictions of quarl zone properties of swirling pulverised coal flames. *Proc. Combust. Inst.*, 1990, **23**, 949-955.
4. **Islam, A. K. M. S. and Hossain, M.** Prediction of local species concentration in an axisymmetric furnace. *J. Energy Heat and Mass Transfer*, 1996, **18**, 141-146.
5. **Peters, N.** Laminar flamelet models in nonpremixed turbulent combustion. *Prog. Energ. Combust. Sci.*, 1984, **10**, 319-339.
6. **Peters, N.** Laminar flamelet concepts in turbulent combustion. *Proc. Combust. Inst.*, 1986, **21**, 1231-1250.
7. **Bilger, R. W.** Conditional moment closure for turbulent reacting flows. *Physics of Fluids A*, 1993, **5(2)**, 436-444.
8. **Pope, S. B**. PDF methods for turbulent reactive flows. *Prog. Energ. Combust. Sci.*, 1985, **11**, 119-192.
9. **Pope, S. B.** Computations of turbulent combustion: progress and challenges. *Proc. Combust. Inst.*, 1990, **23**, 591-612.

10. **Kim, S. H. and Huh, K. Y.** Use of the conditional moment closure model to predict NO formation in a turbulent CH_4/H_2 flame over a bluff-body. *Combust. Flame,* 2002, **130**, 94-111.
11. **Masri, A. R**. Computation of bluff-body stabilized jets and flames. Proceedings of 5^{th} International Workshop on Measurements and Computation of Turbulent Nonpremixed Flames, Delft, The Netharlands. http://www.ca.sandia.gov/TNF (2000) section 3.
12. **Dally, B. B. Masri, A. R., Barlow, R. S. and Fiechtner, G. J.** Instantaneous and mean compositional structure of bluff-body stabilised nonpremixed flames. *Combust. Flame,* 1998, **114**, 119-148.
13. **Masri, A. R.**, Data-base available from the department of Aerospace, Mechanical and Mechatronic Engineering, The university of Sydney, Australia. http://www.aeromech.usyd.edu.au/thermofluids.
14. **Dally, B. B., Fletcher, D. F. and Masri, A. R.** Flow and mixing fields of turbulent bluff-body jets and flames. *Combust. Theor. Model,* 1998, **2**, 193-219.
15. **Merci, B., Dick, E., Vierendeels, J., Roekaerts, D. and Peeters, T. W. J.**, Application of a new cubic turbulence model to piloted and bluff-body diffusion flames. *Combust. Flame,* 2001, **126**, 1533-1556.
16. **Li, G., Naud, B. and Roekaerts, D.**, Numerical investigation of a bluff-body stabilised nonpremixed flame with differential Reynolds-stress models. *Flow Turbul. Combust.*, 2003, **70**, 211-240.
17. **Yan, J., Thiele, F. and Buffat, M.** A turbulence model sensitivity study for CH_4/H_2 bluff-body stabilized flames. *Flow Turbul. Combust*., 2004, **73**, 1-24.
18. **Hossain, M. and Malalasekera W.** Numerical study of bluff-body flame structures using laminar flamelet model. *Proc. Instn Mech. Engnrs, Part A: J. Power and Energy,* 2005, **219**, 361-370.
19. **Hossain, M. and Malalasekera, W.** Modelling of a bluff body stabilised CH_4/H_2 flames based on a laminar flamelet model with emphasis on NO prediction. *Proc. Instn Mech. Engnrs, Part A: J. Power and Energy 2003*, **217**, 201-210.

20. **Hossain, M., Jones, J. C. and Malalasekera, W.** Modelling of a bluff-body nonpremixed flame using a coupled radiation/flamelet combustion model. *Flow Turbul Combust*., 2001; **67**, 217-234.
21. **Muradoglu, M., Liu, K. and Pope, S. B**. PDF modelling of a bluff-body stabilized turbulent flame. Combustion and Flame 2003; 132: 115-7.
22. Liu, K., Pope, S., B. and Caughey, D. A., Calculations of bluff-body stabilised flames using a joint probability density function model with detailed chemistry.
23. **Warnatz, J., Mass, U. and Dibble, R. W.** Combustion: Physical and Chemical fundamentals, modelling and simulation, experiments, pollutant formation. Berlin: Springer-Verlag; 1996.
24. **Rogg, B.** RUN-1DL: The Laminar Flame and Flamelet Code, 1995.
25. **Bilger, R. W.** Structure of turbulent nonpremixed flames. *Proc. Combust. Inst.*, 1988, **22**, 475-488.
26. **Peters, N.** Flame Calculations with Reduced Mechanisms-an outline. In Reduced Kinetic Mechanisms for Applications in Combustion Systems (Eds N. Peters and B. Rogg) 1993, Ch. 1, pp. 3-14 (Springer-Verlag, Berlin).
27. **Barlow, R. S, Dibble, R. W., Lucht, R. P. and Chen J-. Y.** Effect of Damkohler number on superequilibrium OH concentration in turbulent nonpremixed jet flames. *Combust. Flame*, 1990, **82**, 235-251.
28. **Drake, M. C. and Blint, R. J**. Structure of laminar opposed flow diffusion flames with $CO/H_2/N_2$ fuel. *Combust. Sci. and Technol*, 1988, **61**, 187-224.

List of Figures:

Figure 11: Radial profiles of mass fraction of CO_2. ● measurement [12]; ——— laminar flamelet; - - - - - - - flame sheet; -·-·-·-·- equilibrium; –··–··– constrained equilibrium.

Figure 12: Radial profiles of mass fraction of CO. ● measurement [12]; ——— laminar flamelet; - - - - - - - flame sheet; -·-·-·-·- equilibrium; –··–··– constrained equilibrium.

Figure 13: Radial profiles of mass fraction of OH. ● measurement [12]; ——— laminar flamelet; - - - - - - - flame sheet; -·-·-·-·- equilibrium; –··–··– constrained equilibrium.

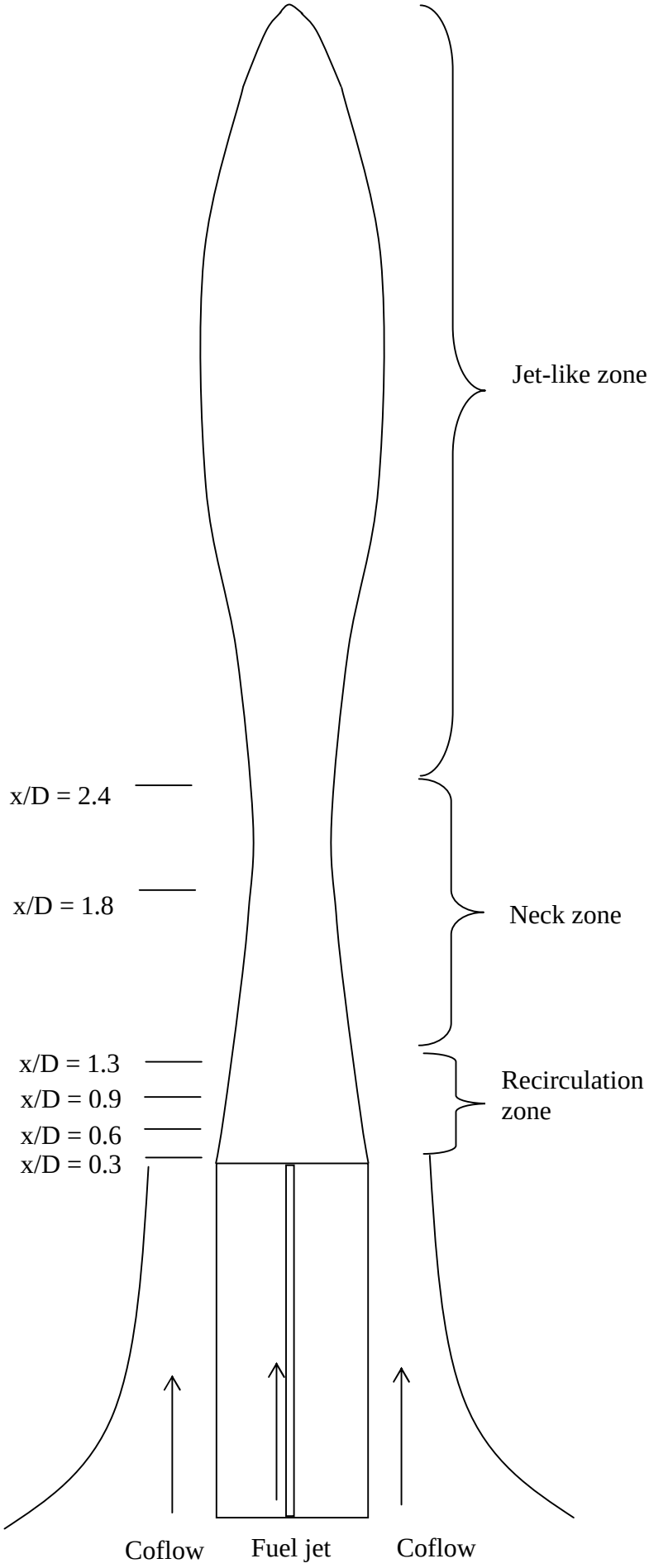

Figure 1: Schematic drawing of a bluff body combustor and measuring locations

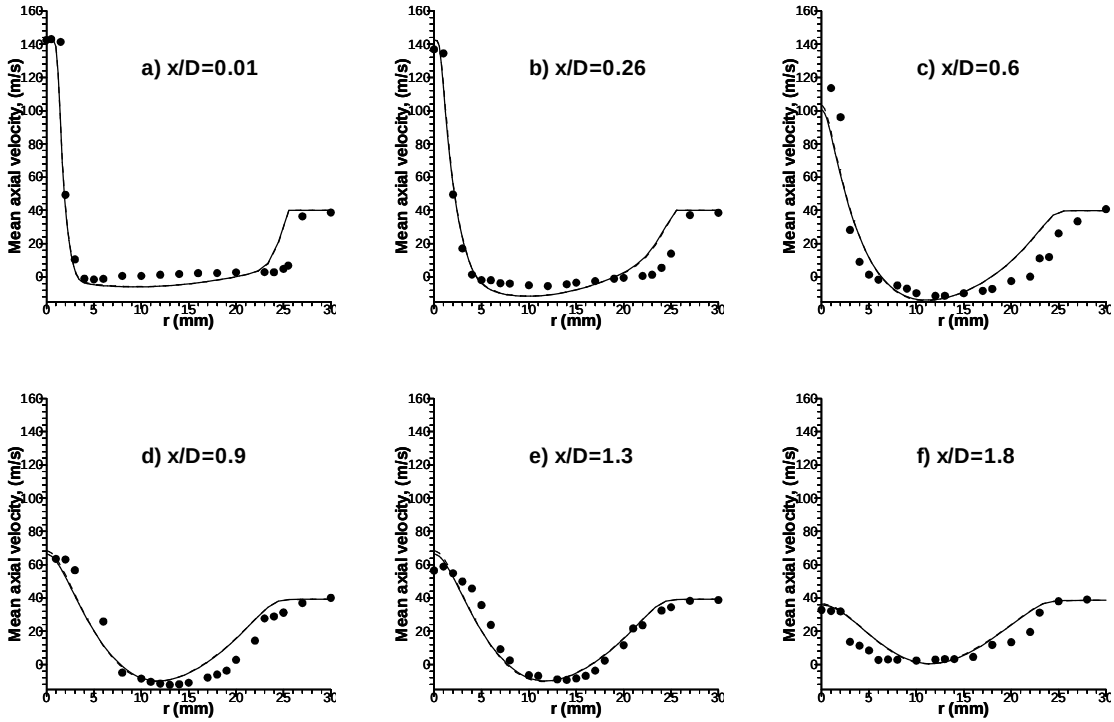

Figure 2: Mean axial velocity profile. ● measurement [12]; ——— laminar flamelet model with 99x89 grid; - - - - - - - laminar flamelet model with 217x197 grid.

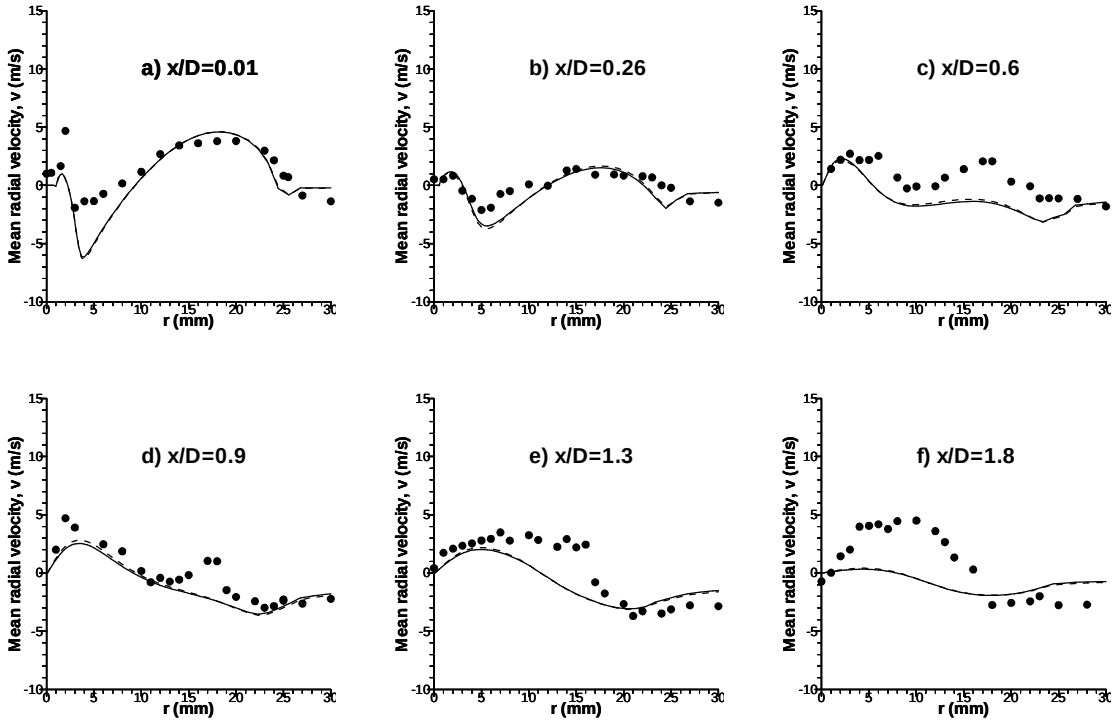

Figure 3: Mean radial velocity profile. ● measurement [12]; ——— laminar flamelet model with 99x89 grid; ------- laminar flamelet model with 217x197 grid.

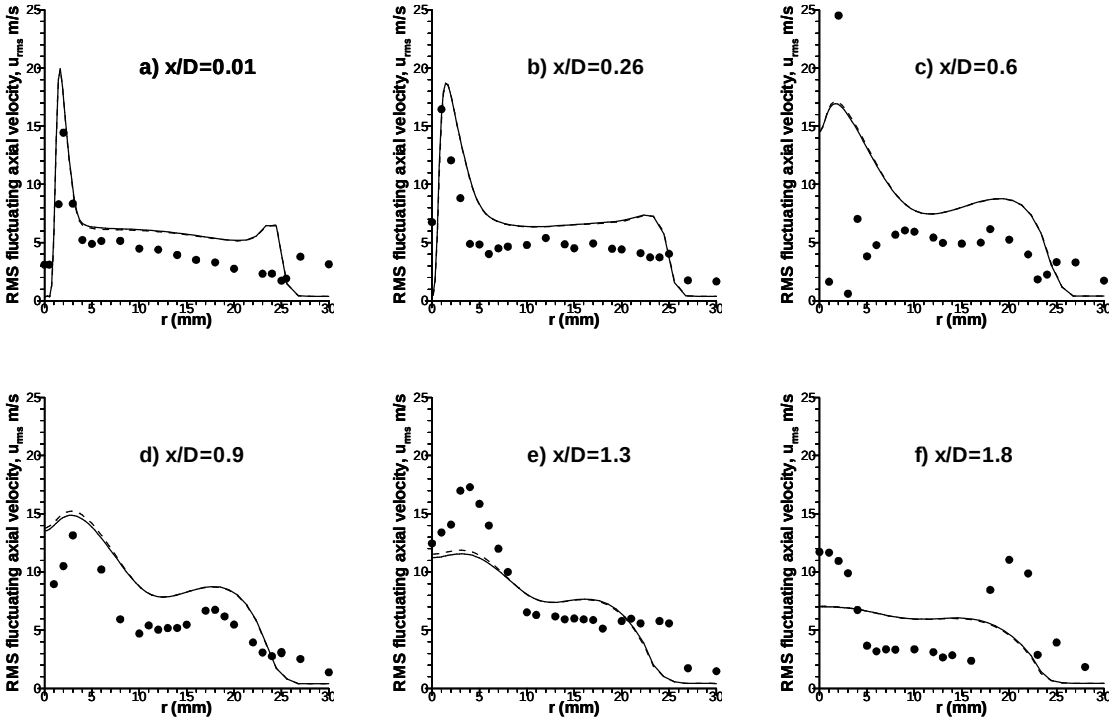

Figure 4: Axial velocity fluctuations (rms of axial velocity). ● measurement [12]; ——— laminar flamelet model with 99x89 grid; - - - - - - - laminar flamelet model with 217x197 grid.

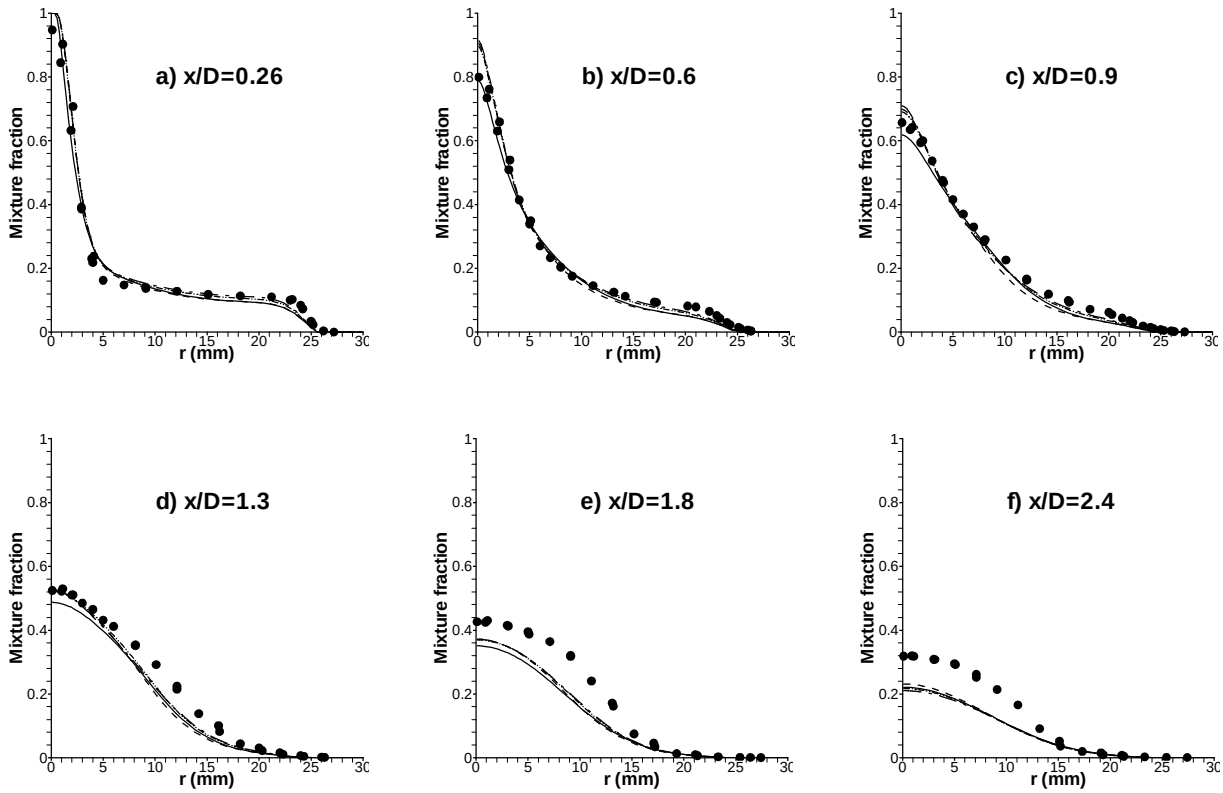

Figure 5: Radial profiles of mixture fraction. ● measurement [12]; ——— laminar flamelet; - - - - - - - flame sheet; -·-·-·-·- equilibrium; —·—·— constrained equilibrium.

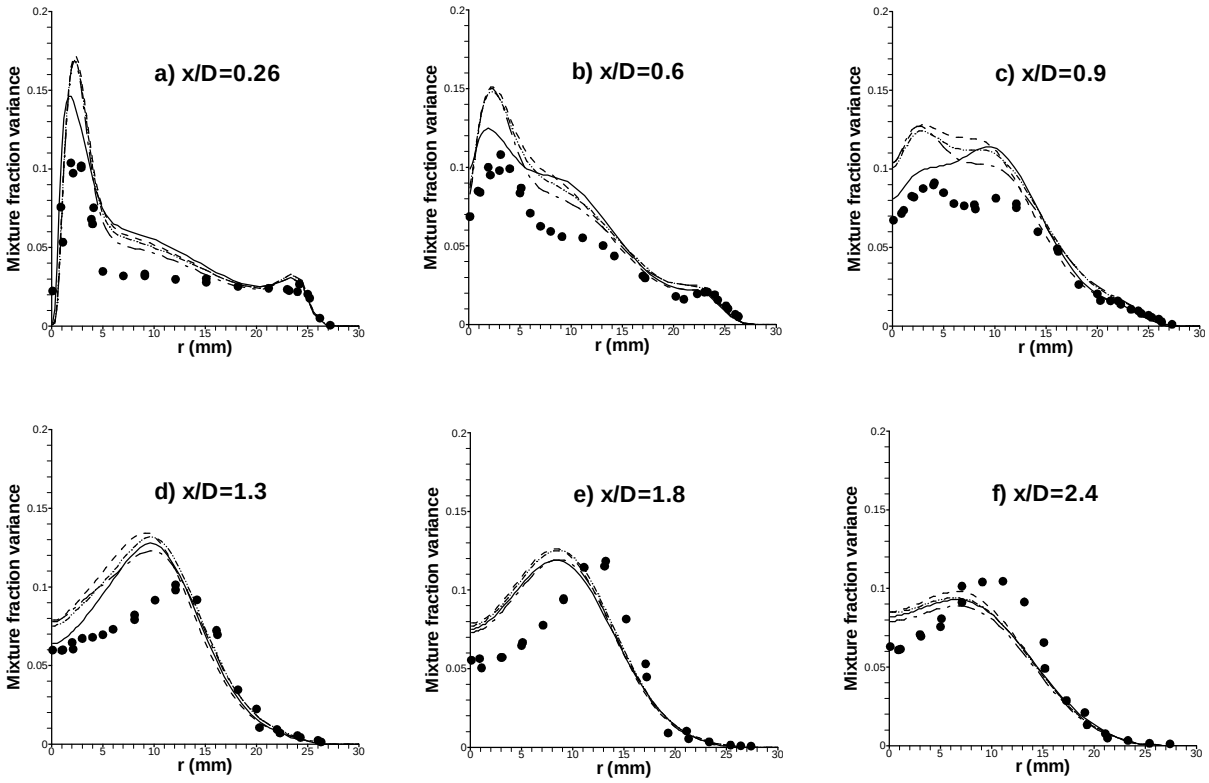

Figure 6: Radial profiles of mixture fraction variance. ● measurement [12]; ——— laminar flamelet; - - - - - - - flame sheet; - · - · - · - equilibrium; — · — · — constrained equilibrium.

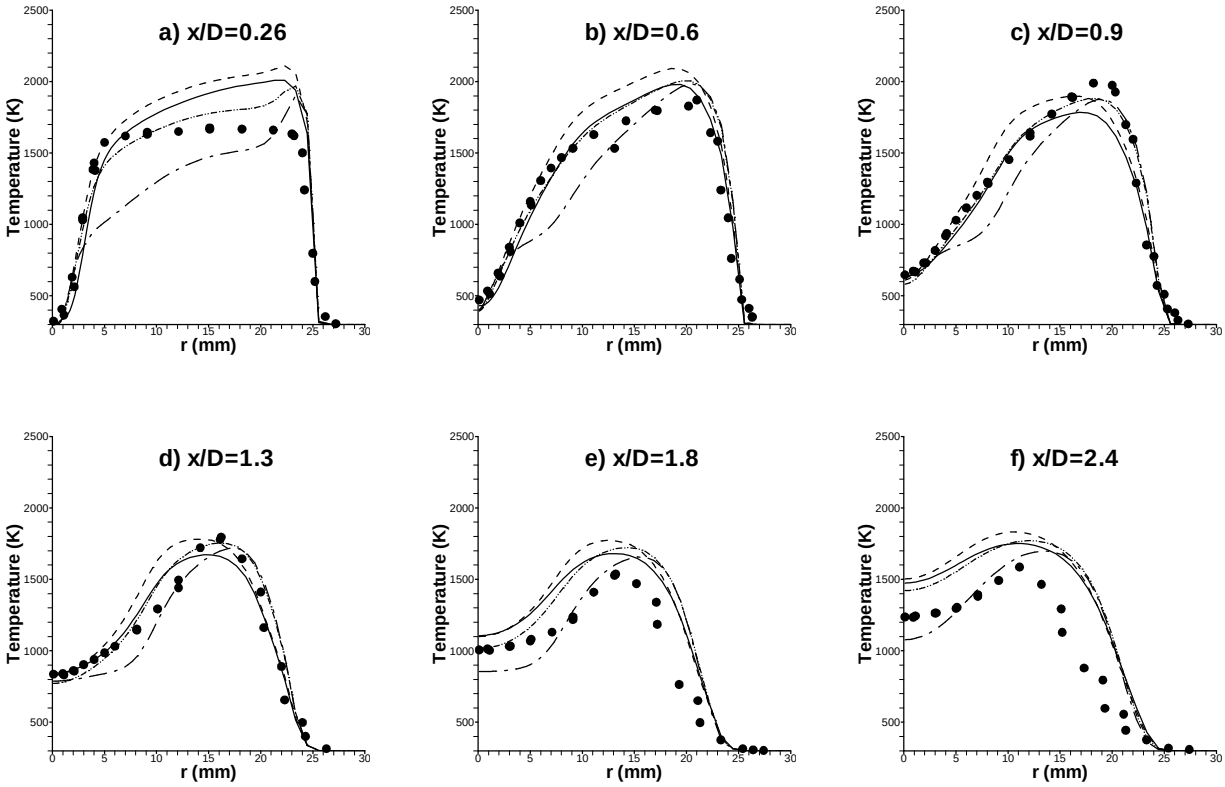

Figure 7: Radial profiles of temperature. ● measurement [12]; ——— laminar flamelet; - - - - - - - flame sheet; -·-·-·-·- equilibrium; —·—·— constrained equilibrium.

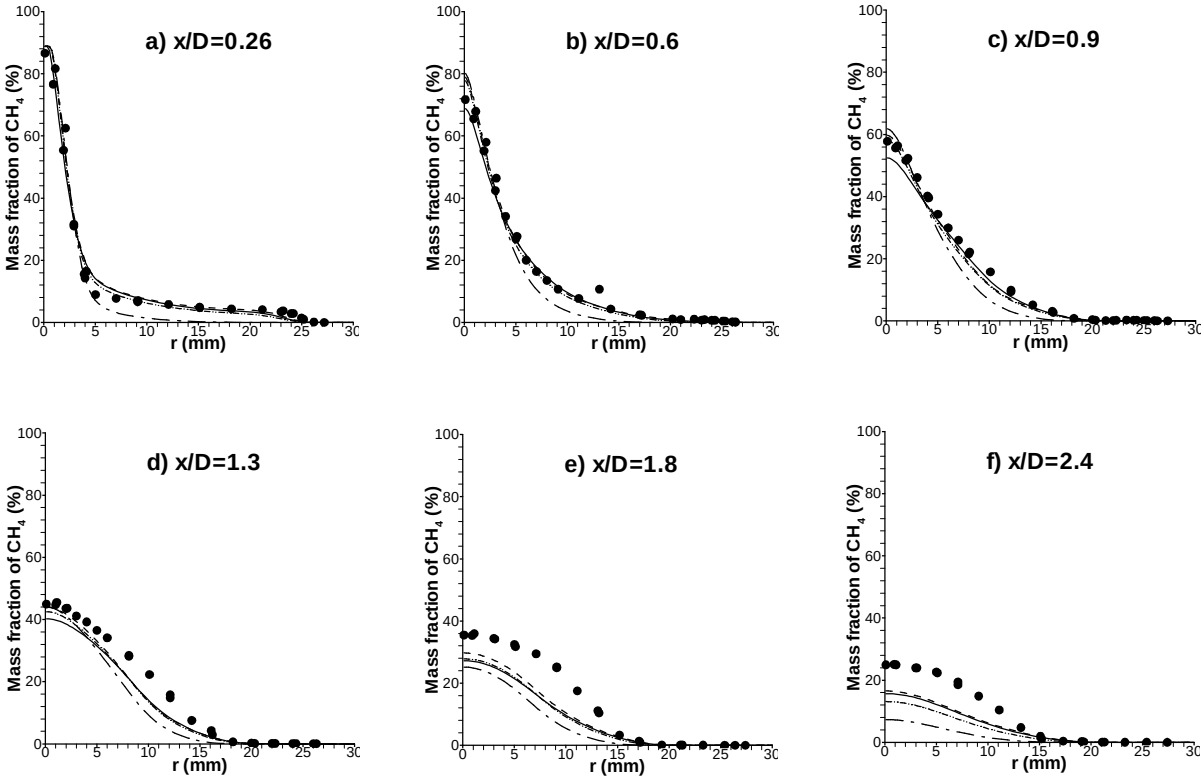

Figure 8: Radial profiles of mass fraction of CH_4. ● measurement [12]; ——— laminar flamelet; - - - - - - - flame sheet; -·-·-·-·- equilibrium; —·—·— constrained equilibrium.

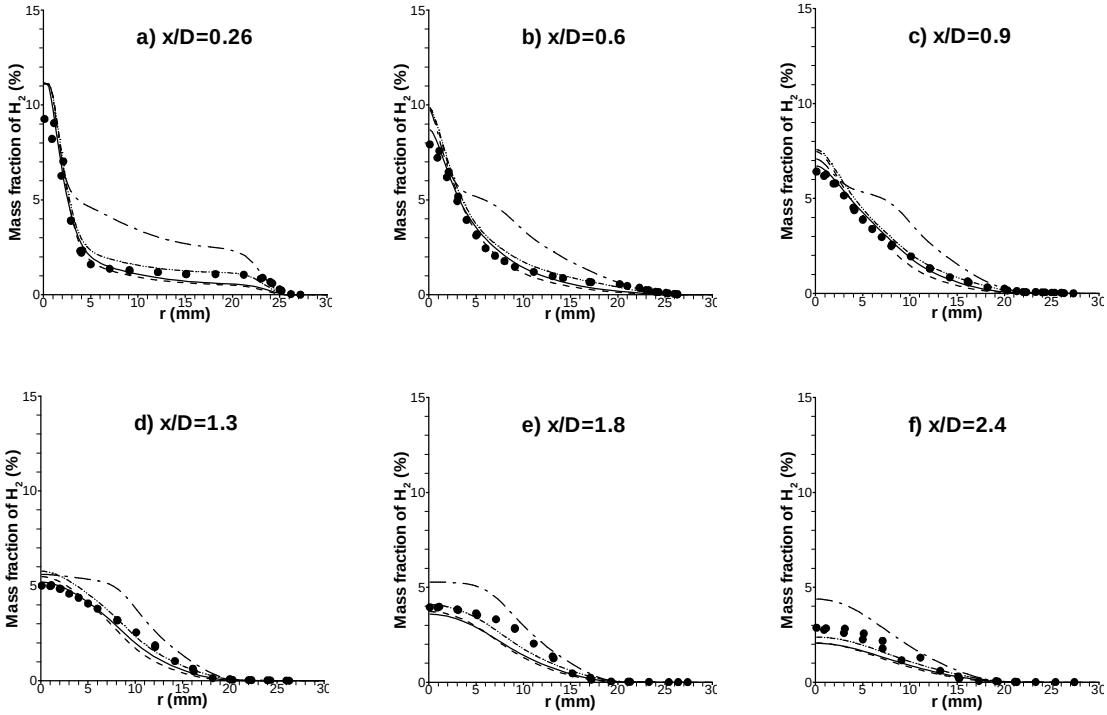

Figure 9: Radial profiles of mass fraction of H_2. ● measurement [12]; ——— laminar flamelet; - - - - - - - flame sheet; -·-·-·-·- equilibrium; —·—·— constrained equilibrium.

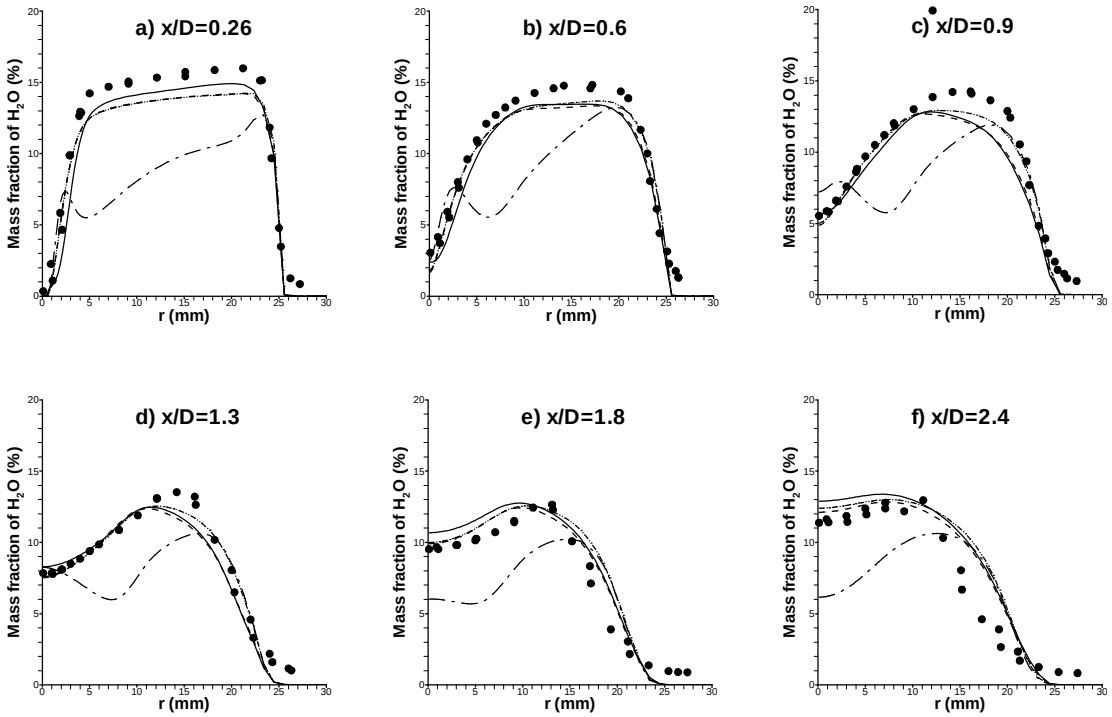

Figure 10: Radial profiles of mass fraction of H_2O. ● measurement [12]; ——— laminar flamelet; - - - - - - - flame sheet; -·-·-·-·- equilibrium; —·—·— constrained equilibrium.

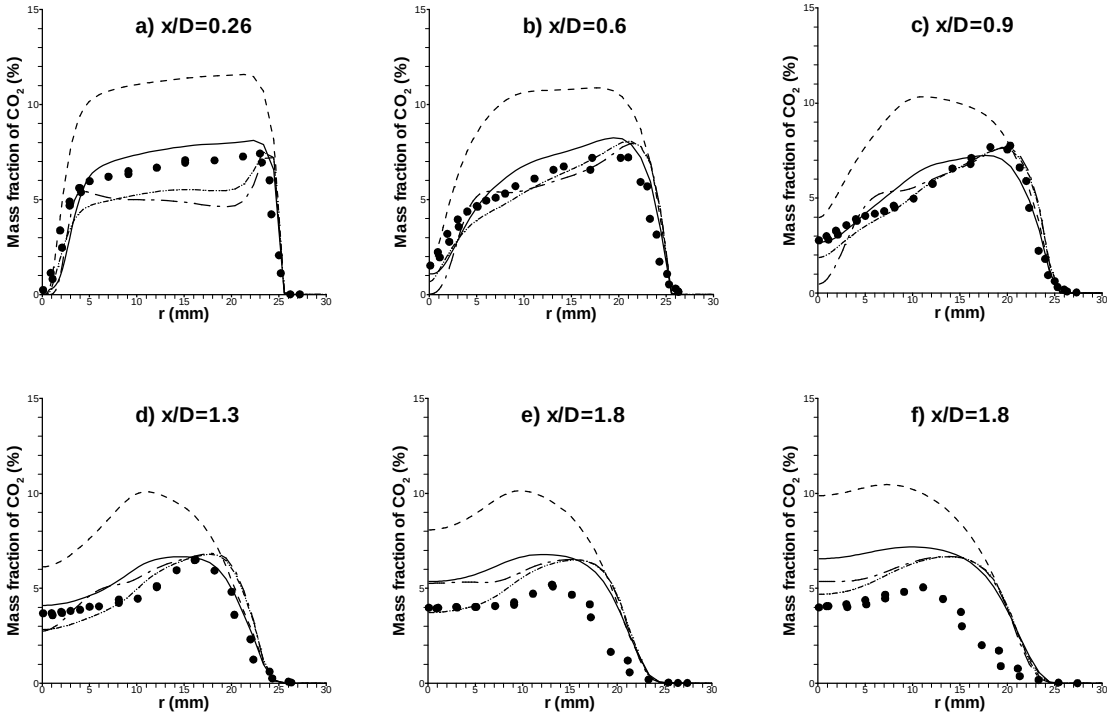

Figure 11: Radial profiles of mass fraction of CO_2. ● measurement [12]; ——— laminar flamelet; - - - - - - - flame sheet; -·-·-·-·- equilibrium; —·—·— constrained equilibrium.

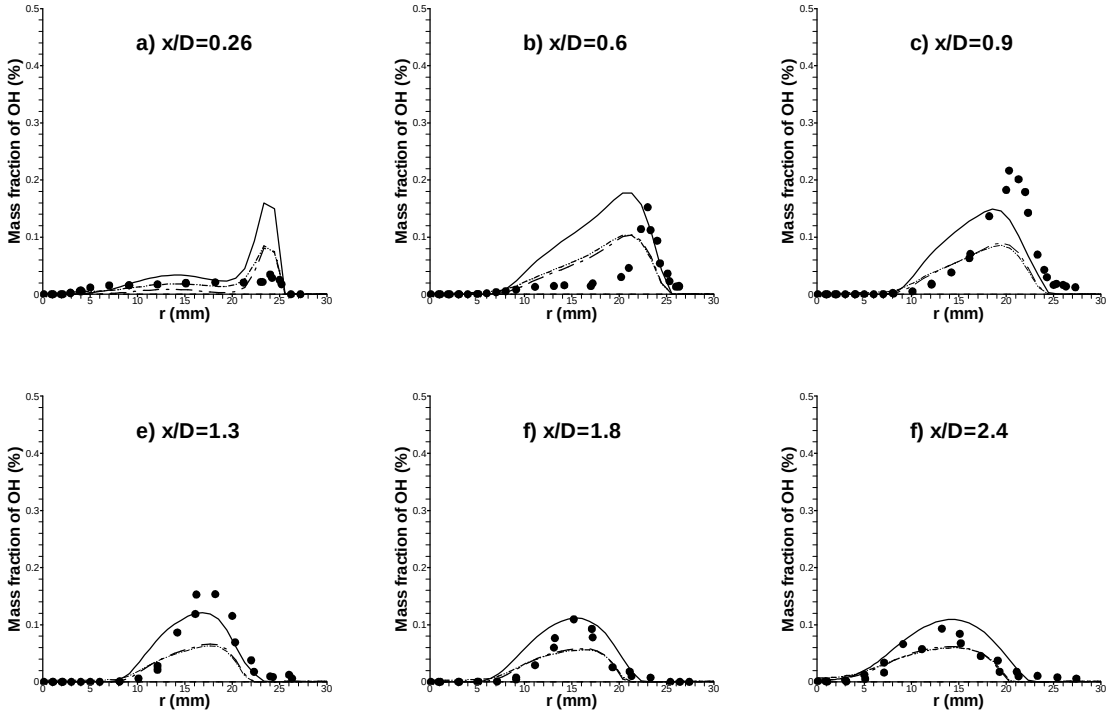

Figure 12: Radial profiles of mass fraction of OH. ● measurement [12]; ——— laminar flamelet; - - - - - - - flame sheet; -·-·-·-·- equilibrium; —·—·— constrained equilibrium.

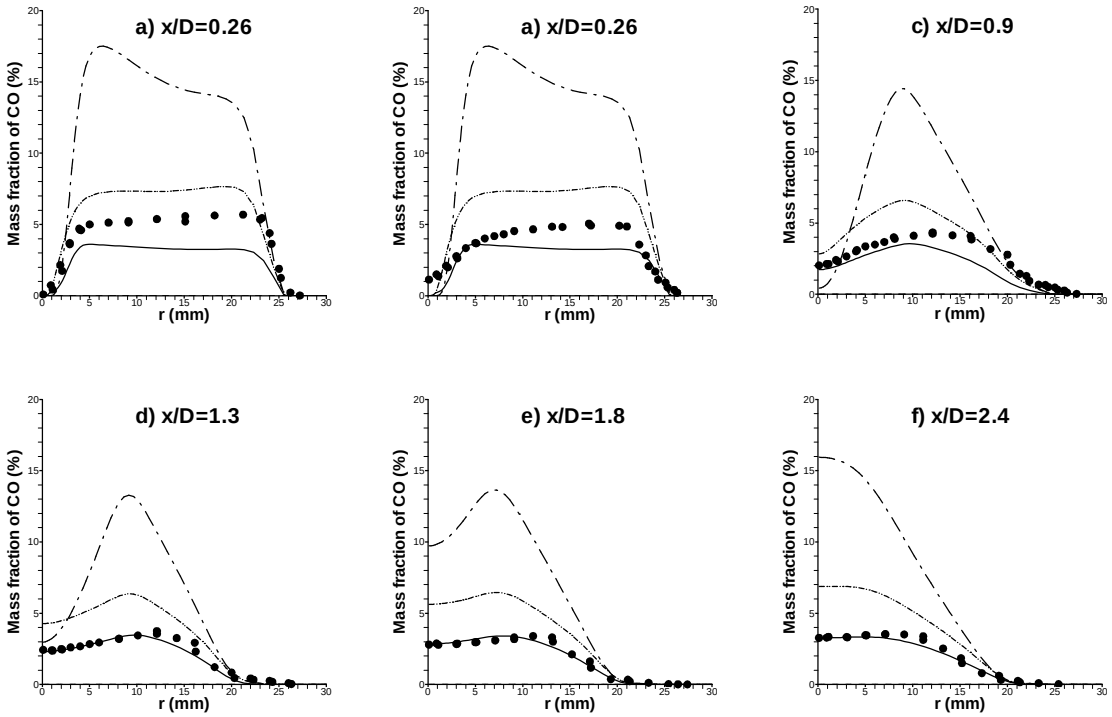

Figure 13: Radial profiles of mass fraction of CO. ● measurement [12]; ——— laminar flamelet; - - - - - - - flame sheet; -·-·-·-·- equilibrium; —·—·— constrained equilibrium.